DOI: 10.1002/ejic.201001210

Four New Compounds Constructed from Bis-Antimony-Capped Keggin Polyoxoanions $\{PMo_{12}Sb_2O_{40}\}$ and Different Coordination Fragments

Li-Na Xiao,[a] Yu Peng,[a] Yan Wang,[a] Jia-Ning Xu,[a] Zhong-Min Gao,[a] Ya-Bing Liu,[a] Da-Fang Zheng,[a] Xiao-Bing Cui,*[a] and Ji-Qing Xu*[a]

Keywords: Antimony / Molybdenum / Polyoxometalates / Heteropolyanions / Coordination modes / Transition metals

Four new heteropolyanions $\{[PMo_{12}Sb_2O_{40}][Cu(Im)_2]_2\}\cdot Im$ (**1**), $\{[PMo_{12}Sb_2O_{40}][(Cd(Phen)_2)_2Cl]\}$ (**2**), $[Cu(Phen)_2]_2[PMo_{12}Sb_2O_{40}]$ (**3**) and $[Cd(bpy)_4(H_2O)_2][PMo_{12}Sb_2O_{40}]\cdot bpy\cdot 2H_2O$ (**4**) (Im = imidazole, Phen = 1,10-phenanthroline, bpy = 4,4′-bipyridine) have been synthesized and characterized by IR, UV/Vis spectrophotometry, X-ray photoelectron spectroscopy, powder XRD analyses and elemental analyses. Single-crystal X-ray diffraction analyses revealed that these four compounds represent examples of compounds based on the bis-antimony-capped Keggin polyoxoanion $\{PMo_{12}Sb_2O_{40}\}$ and different transition-metal coordination complexes. Compound **1** exhibits a novel 1D chain structure, compound **2** is the first example of an extended structure constructed from polyoxoanions, transition-metal coordination complexes and halide ions and compounds **3** and **4** are supramolecular structures constructed from $\{PMo_{12}Sb_2O_{40}\}$ polyoxoanions and different transition-metal coordination fragments.

Introduction

It has been widely recognized that polyoxometallates (POMs) exhibit a variety of structures and properties that make them useful in catalysis, materials science and medicine.[1–6] This class of metal–oxygen clusters is formed from early transition metals of groups V and VI (V, Nb, Ta, Mo and W) in their highest oxidation states (e.g., V^{5+}, W^{6+}).[1] A recent new advance in the burgeoning field of POM chemistry is the large number of hybrid compounds constructed from a combination of POMs and transition-metal cations or transition-metal coordination complexes (TMCs) that have been obtained. These can be divided into two groups: i. 1D, 2D and even 3D extended structures, for the spherical surfaces of POMs provide a better opportunity for forming covalent bonds with transition-metal cations or TMCs.[7–10] ii. Supramolecular structures constructed from POMs and TMCs through non-covalent interactions.[11] An intelligent choice of POMs and transition-metal cations or TMCs may yield materials with fascinating structures and desirable properties. The diversity of POMs and transition-metal cations or TMCs has led to a wide array of functional organic–inorganic hybrid materials.

Up to now, most of the existing POM species have already been used as building blocks to be connected to different transition-metal cations or TMCs to form extended structures, including Keggin and Dawson POMs. In 2006 and then in 2010, we prepared a new POM species: bis-antimony-capped Keggin polyoxoanion $\{PMo_{12}Sb_2O_{40}\}$ with two different configurations: pseudo-Keggin and α-Keggin.[12] The only difference in the two is the central PO_4^{3-} unit, which in the α-Keggin configuration exhibits a tetrahedral geometry whereas in the pseudo-Keggin configuration it exhibits a cubic geometry with all eight oxygen atoms half occupied.[12] We then successfully combined different TMCs with the new POM species to form three novel hybrid materials with extended structures.[9f] Hitherto, only these three compounds based on the $\{PMo_{12}Sb_2O_{40}\}$ POM have been synthesized, compared with an abundance of compounds based on Keggin, Dawson or other POMs. It is believed that many such compounds could be synthesized and thus we have directed our investigations towards the development of further compounds based on this new POM species $\{PMo_{12}Sb_2O_{40}\}$. The three previously reported compounds are all based on aliphatic organic ligands, so we have tried to extend the research on POM $\{PMo_{12}Sb_2O_{40}\}$ to compounds with aromatic organic ligands.

As part of the continuing work on this system, we have successfully synthesized four new hybrids based on aromatic organic ligands, two of which exhibit extended structures based on the α-Keggin configuration of $\{PMo_{12}Sb_2O_{40}\}$ and the other two exhibit novel supramolecular structures based on the pseudo-Keggin configuration. Thus, we have found two new examples of extended structures based on $\{PMo_{12}Sb_2O_{40}\}$, $\{[PMo_{12}Sb_2O_{40}][Cu(Im)_2]_2\}\cdot Im$ (**1**) and $\{[PMo_{12}Sb_2O_{40}][(Cd(Phen)_2)_2Cl]\}$ (**2**) (Im = imidazole, Phen = 1,10-phenanthroline), and also

[a] College of Chemistry and State Key Laboratory of Inorganic Synthesis and Preparative Chemistry, Jilin University, Changchun, Jilin 130023, P. R. of China
E-mail: cuixb@mail.jlu.edu.cn
xjq@mail.jlu.edu.cn

Supporting information for this article is available on the WWW under http://dx.doi.org/10.1002/ejic.201001210.

the first examples of supramolecular structures based on the polyoxoanion $\{PMo_{12}Sb_2O_{40}\}$, $[Cu(Phen)_2]_2[PMo_{12}Sb_2O_{40}]$ (**3**) and $[Cd(bpy)_4(H_2O)_2][PMo_{12}Sb_2O_{40}]\cdot bpy\cdot 2H_2O$ **(4)** (bpy = 4,4′-bipyridine).

Results and Discussion

As with all hydrothermal syntheses, the reaction products can be very sensitive to the initial reaction conditions. Small changes in temperature, mol ratios and reaction time can have a great effect on the yields and phase purity of products.

Up to now, only seven hybrids based on $\{PMo_{12}Sb_2O_{40}\}$ POMs and TMCs have been reported. All these compounds were prepared by hydrothermal reactions by our group and the conditions for their preparation are displayed in Scheme 1. The yields of the seven compounds are comparable (from 60–85%), except for compound **7**, which was prepared in low yield (21%). The previously reported hybrids $[PMo_{12}Sb_2O_{40}][Cu(enMe)_2]\cdot 4H_2O$ (**5**), $[PMo_{12}Sb_2O_{40}][Ni(enMe)_2]\cdot 4H_2O$ (**6**) and $[PMo_{12}Sb_2O_{40}][Cu(en)_2]\cdot H_3O\cdot H_2O$ (**7**) (enMe = 1,2-diaminopropane, en = ethylenediamine) based on the anion $\{PMo_{12}Sb_2O_{40}\}$ with the pseudo-Keggin configuration were synthesized by using $[(NH_4)_6Mo_7O_{24}]\cdot 4H_2O$, H_3PO_4, $Sb_2O_3/SbCl_3$, $CuAc_2\cdot H_2O/NiCl_2\cdot 6H_2O$ and different aliphatic organic ligands as starting materials.[9f] We first synthesized the hybrids **1** and **2** based on the anion $\{PMo_{12}Sb_2O_{40}\}$ with the α-Keggin configuration by using $[(NH_4)_3PMo_{12}O_{40}]\cdot xH_2O$, $H_2C_2O_4\cdot 2H_2O$, Sb_2O_3, $CuCl_2\cdot 2H_2O/CdCl_2\cdot 2.5H_2O$ and different aromatic organic ligands as the starting materials. Thus, we speculated that perhaps the the main reason for the two different configurations is the different starting materials. However, we then prepared compounds **3** and **4**, which are based on the pseudo-Keggin configuration but were synthesized by using analogous starting materials to those used for the preparation of compounds **1** and **2**. The syntheses of compounds **3** and **4** demonstrate that our speculation was incorrect.

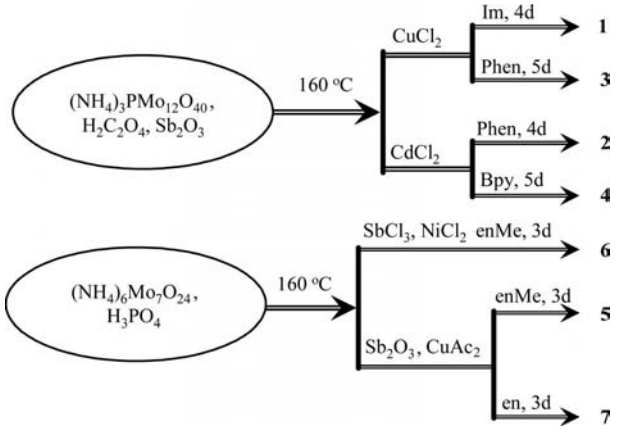

Scheme 1. Summary of the reactions leading to compounds **1**–**7**.

We carefully explored the reactivity of the P/Mo/Sb/M (M = Cu or Cd)/aromatic organic ligand system under hydrothermal conditions. The pH value plays a key role in the preparation of **1**–**4**. Only when the pH value was 4 did we succeed in synthesizing **1** and **3**, only when the pH value was 4.5 did we succeed in synthesizing **2** and only when the pH value was 5.5 did we succeed in synthesizing **4**. Many parallel experiments demonstrated that syntheses at pH values deviating from 4, 4.5 or 5.5 yielded nothing or undetermined powders. Compound **5** was synthesized at a pH value of 4.5, compound **6** at a pH value of 7.5 and compound **7** at a pH value of 5. From these experiments we could conclude that the compounds based on $\{PMo_{12}Sb_2O_{40}\}$ and TMCs can be easily synthesized under weakly acidic conditions, especially when using aromatic organic ligands.

We also tried to synthesize **1**–**4** with $SbCl_3$ instead of Sb_2O_3 under the same conditions, but this was not successful. In addition, we tried to synthesize analogous compounds of **2** and **3** under the same conditions with 2,2′-bpy replacing Phen. Unfortunately, we did not achieve this goal.

It was very interesting that compound **2** contains a chloride ion, however, no chloride ions were included in **1**, **3** or **4**. The reason for this remains unclear.

Crystal Structure of 1

Single-crystal X-ray diffraction analysis revealed that the asymmetric unit of **1** contains the polyoxoanion $[PMo_{12}Sb_2O_{40}]^{2-}$ with the α-Keggin configuration, two $[Cu(Im)_2]^+$ TMCs and one Im ligand. The polyoxoanion $[PMo_{12}Sb_2O_{40}]^{2-}$ contains the well-known α-Keggin core $\{PMo_{12}O_{40}\}$ with two antimony atoms capping the two opposite cavities. The P–O, Mo–O and Sb–O distances in **1** are all comparable to those of the $\{PMo_{12}Sb_2O_{40}\}$ POMs reported previously.[9f,12] The bond valence sums (BVSs) for the molybdenum and antimony atoms were calculated by using parameters provided by Brown.[13] The results give an average value of 5.60 for Mo(1)–Mo(12) and of 2.72 for Sb(1)–Sb(2), which reveals that the oxidation state of five of the molybdenum atoms is +5 and the oxidation state of the remaining seven molybdenum atoms of $\{PMo_{12}Sb_2O_{40}\}$ is +6 and that of the antimony atoms is +3. Thus, the formula of $\{PMo_{12}Sb_2O_{40}\}$ is $[PMo^{V}_{5}Mo^{VI}_{7}Sb^{III}_{2}O_{40}]^{2-}$.

Note that there are two crystallographically different copper ions in **1**: $Cu(1)^+$ and $Cu(2)^+$. Each Cu^+ ion receives contributions from the two nitrogen atoms of Im with the Cu–N bond lengths being 1.862(6)–1.873(6) Å. They also each receive contributions from two oxygen atoms from two neighbouring POMs $[PMo_{12}Sb_2O_{40}]^{2-}$, one of which is a terminal oxygen of a POM with Cu–O distances of 2.920(6)–3.008(5) Å and the other is a bridging oxygen from the neighbouring POM with Cu–O distances of 2.773(6)–3.068(6) Å. The two $[Cu(1)(Im)_2]^+$ TMCs, which act as double bridges, are both located on the "left" of a $[PMo_{12}Sb_2O_{40}]^{2-}$ POM, whereas the two $[Cu(2)(Im)_2]^+$ TMCs, which also act as double bridges, are both located on the "right" of the $[PMo_{12}Sb_2O_{40}]^{2-}$ POM. Thus, the

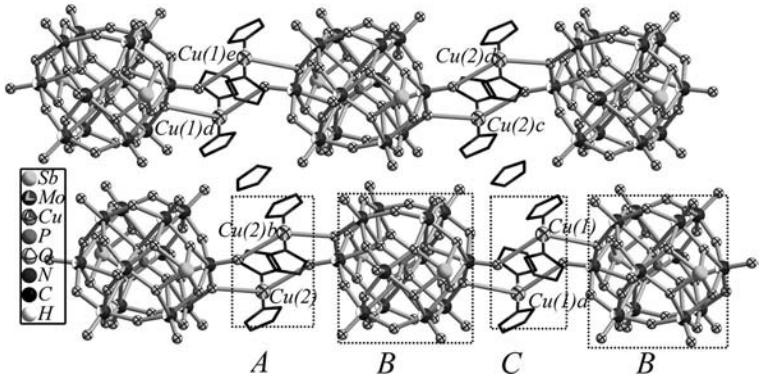

Figure 1. Combined ball-and-stick and wire representation of the π···π interactions between the dissociated Im ligands and the Im ligands coordinated to the copper ions from two adjacent chains in compound **1**. Symmetry code: a: 1 – *x*, 1 – *y*, –*z*; b: –*x*, –*y*, 1 – *z*; c: 1 + *x*, 1 + *y*, *z*; d: 1 – *x*, 1 – *y*, 1 – *z*; e: *x*, *y*, 1 + *z*.

$[Cu(1)(Im)_2]^+$ and $[Cu(2)(Im)_2]^+$ double bridges interconnect neighbouring polyoxoanions $[PMo_{12}Sb_2O_{40}]^{2-}$ through Cu–O bonds to yield an unusual infinite $[PMo_{12}Sb_2O_{40}]$-$[Cu(Im)_2]$ neutral chain structure (as shown in Figure 1). The most remarkable feature of **1** is that the anion $[PMo_{12}Sb_2O_{40}]^{2-}$ is utilized as a multidentate chelating ligand, coordinating to four $[Cu(Im)_2]^+$ TMCs through terminal and bridging oxygen atoms to yield an unprecedented 1D chain structure.

Note that the distance between the two Cu(1) atoms of the $[Cu(1)(Im)_2]^+$ double bridge is 4.504(2) Å, whereas the distance between the two Cu(2) atoms of the $[Cu(2)(Im)_2]^+$ double bridge is 4.176(2) Å. The two Cu(1) atoms interact with the POMs through oxygen atoms with bond lengths of 3.008(5)–3.068(6) Å, whereas the two Cu(2) atoms interact with the POMs through oxygen atoms with bond lengths of 2.773(6)–2.920(6) Å. Thus, the infinite chain constructed from the POMs and two different double bridges are linked in an –ABCB– fashion, as shown in Figure 1.

In addition, there still exists dissociated Im in **1**. The dissociated Im ligands show strong π···π interactions with the Im ligands (N3 ligand) coordinated to the Cu(1) ions with interplanar distances of about 3.10 Å. The dissociated Im ligands also show strong π···π interactions with the Im ligands (N5 ligand) coordinated to the Cu(2) ions from an adjacent infinite chain with interplanar distances also of about 3.10 Å. Thus, the π···π interactions between the dissociated Im and the coordinated Im from adjacent chains connect the chains to form a supramolecular layer structure, as shown in Figure 1.

Detailed analysis shows that there exist extensive hydrogen-bonding interactions between the carbon atoms of the Im ligands and the oxygen atoms of the polyoxoanions $[PMo_{12}Sb_2O_{40}]^{2-}$. These hydrogen bonds are listed in Table S1. In addition, there also exist complex N–H···O interactions (also listed in Table S1) between the nitrogen atoms of the Im ligands and the oxygen atoms of the polyoxoanions $[PMo_{12}Sb_2O_{40}]^{2-}$. These complex hydrogen bonds increase the stability of the structure of compound **1**.

Crystal Structure of 2

The asymmetric unit of **2** consists of half of a $[PMo_{12}Sb_2O_{40}]^{3-}$ unit with the α-Keggin configuration and a $[Cd(Phen)_2Cl_{0.5}]^{1.5+}$ TMC. The $[PMo_{12}Sb_2O_{40}]^{3-}$ is identical to that of compound **1**, the only differences being in the bond lengths and angles. Note that the antimony atoms in **2** are disorderedly distributed about two positions with equivalent occupancy factors of 0.5. Thus, the POMs are connected by the disordered antimony atoms to form a pseudo-chain structure along the *c* axis. Such disorder of the capping antimony atoms has been observed previously in $\{SiMo_{12}Sb_2O_{40}\}$.[14] The results of the BVSs (Table S2) reveal that the formula of the $\{PMo_{12}Sb_2O_{40}\}$ in **2** is $[PMo^{V}_{6}Mo^{VI}_{6}Sb^{III}_{2}O_{40}]^{3-}$.[13]

An unusual feature of **2** is that it contains a novel $[Cd(Phen)_2Cl_{0.5}]^{1.5+}$ TMC. It is not a simple metal–ligand coordination complex, but contains a chloride ion coordinated to the cadmium centre. The Cd ion is coordinated by the four nitrogen atoms of the two Phen units with bond lengths of 2.31(1)–2.32(1) Å, thereby forming a $[Cd(Phen)_2]^{2+}$ TMC. Two $[Cd(Phen)_2]^{2+}$ TMCs are connected by a chloride ion with Cd–Cl bond lengths of 2.545(3) Å to form a novel dimer formulated as $\{[Cd(Phen)_2]_2Cl\}^{3+}$. Thus, the chloride ion serves as an inorganic bridge joining two $[Cd(Phen)_2]^{2+}$ TMCs to form a novel metal–chloride–ligand coordination complex or a novel metal chloride cluster. As shown in Figure S1, the novel cluster $\{[Cd(Phen)_2]_2Cl\}^{3+}$ exhibits a very beautiful "butterfly" motif.[15]

The most unusual feature of **2** is that the "butterfly" clusters acting as bridges interconnect the $[PMo_{12}Sb_2O_{40}]^{3-}$ POMs to form a novel chain structure, as shown in Figure 2. The cadmium ions of the "butterfly" clusters interact with the terminal oxygen atoms of the $[PMo_{12}Sb_2O_{40}]^{3-}$ POMs with Cd–O bond lengths of 2.889(9) Å. Thus, the Cd–O and Cd–Cl contacts connect the $[Cd(Phen)_2]^{2+}$ TMCs, the chloride ions and the $[PMo_{12}Sb_2O_{40}]^{3-}$ POMs along the *b* axis to form a novel chain structure. To the best of our knowledge, it is the first chain structure synchronously constructed from POMs, TMCs and halide ions.

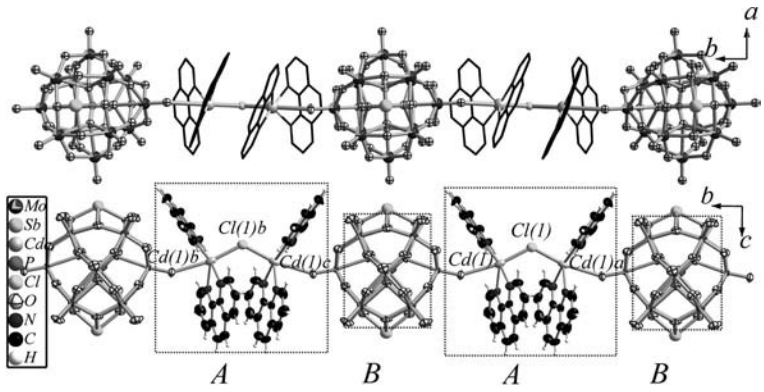

Figure 2. (a) Combined ball-and-stick and wire representation of the 1D chain structure constructed from the $[PMo_{12}Sb_2O_{40}]^{3-}$ POMs and the $\{[Cd(Phen)_2]_2Cl\}^{3+}$ clusters viewed along the *c* axis in compound **2**. (b) Ellipsoid representation of the 1D chain structure viewed along the *a* axis in compound **2**. Symmetry code: a: –0.5 – *x*, 0.5 – *y*, *z*; b: *x*, 1 + *y*, *z*; c: –0.5 – *x*, 1.5 – *y*, *z*.

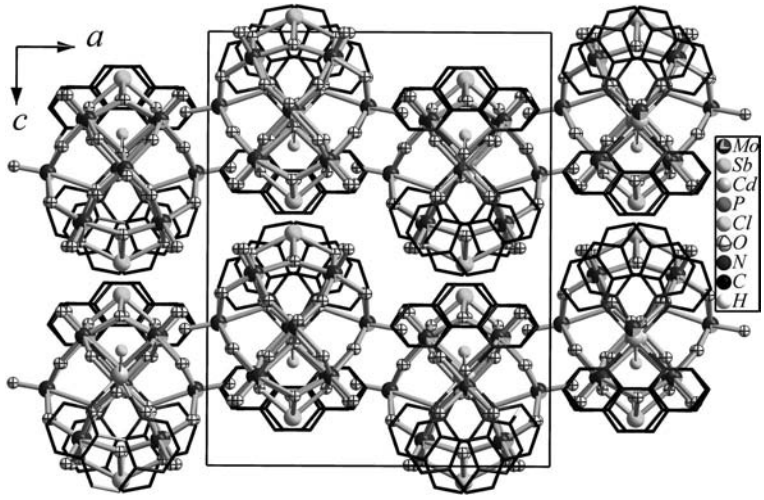

Figure 3. Combined ball-and-stick and wire representation of the packing motif of **2**.

Detailed analysis of the chain structure shows that the chain is straight, which means that the POMs and the "butterfly" clusters are connected in an –ABAB– fashion. The diameter (from Sb1 to Sb2) of the $[PMo_{12}Sb_2O_{40}]^{3-}$ POM is 8.838(4) Å and the diameter (from C6 to the line through C18 and C18d, as shown in Figure S1) of the "butterfly" cluster is about 9.8521 Å, which means that the $[PMo_{12}Sb_2O_{40}]^{3-}$ POM can almost fully overlap the "butterfly" cluster or the "butterfly" cluster can almost fully overlap the $[PMo_{12}Sb_2O_{40}]^{3-}$ POM. If the chain is viewed along the *b* axis, as shown in Figure 3, we find that only the $[PMo_{12}Sb_2O_{40}]^{3-}$ POM or the "butterfly" cluster can be seen.

The packing motif of **2** is shown in Figure 3. The straight chains are packed orderly one by one. Note that the phenol rings of the Phen ligands are all "in" the chain, that is, they do not project from the chain and so there will no π···π interactions between Phen ligands of different chains.

There also exist extensive hydrogen-bonding interactions between the carbon atoms of the Phen ligands and the oxygen atoms of the polyoxoanions $[PMo_{12}Sb_2O_{40}]^{3-}$, as for compound **1**. These hydrogen bonds are listed in Table S1.

Crystal Structure of 3

The asymmetric unit of **3** is constructed from half of a $[PMo_{12}Sb_2O_{40}]^{3-}$ with the pseudo-Keggin configuration and a $[Cu(Phen)_2]^+$ TMC. The central PO_4^{3-} of the $[PMo_{12}Sb_2O_{40}]^{3-}$ in **3** is different to the one in compounds **1** and **2**, exhibiting a cubic geometry with all eight oxygens half occupied. The results of the BVSs (Table S2) reveal that the formula of the $\{PMo_{12}Sb_2O_{40}\}$ in **3** is $[PMo^{V}{}_5Mo^{VI}{}_7Sb^{III}{}_2O_{40}]^{2-}$.[13]

Just as for compounds **1** and **2**, compound **3** contains TMCs, in this case $[Cu(Phen)_2]^+$. However, the role of the TMCs in **3** is totally different to the TMCs in compounds **1** and **2**. The TMCs in **3** show weak interactions with the POMs. Thus, the TMCs here serve only as inorganic counterions. However, detailed analysis reveals an interesting packing motif for **3**.

The Cu(1) ion in **3** exhibits a distorted tetrahedral coordination environment, which is defined by four nitrogen atoms from two Phen units with Cu–N distances of 2.005(6)–2.080(7) Å. Such a coordination environment indicates that the oxidation state of the copper ion is +1. The

dihedral angle between the two Phen planes is about 67.1(1)°, which means that the $[Cu(Phen)_2]^+$ distorted tetrahedron is chiral.

As shown in Figure S2, an unusual feature of **3** is the interaction of two chiral copper TMCs to form a novel chiral dimer through strong π···π interactions between the Phen ligands with an interplanar distance of about 3.50 Å. The distance between the two copper atoms of the two TMCs in the dimer is 7.391(2) Å.

Another unusual feature of **3** is that the dimers in **3** show two different "orientations", as shown in Figure S2. The "left" dimers stack along the *b* axis to form a chain structure and the "right" ones also stack along the *b* axis to form a chain structure. It is interesting that the two chains are arranged in parallel and stack along the *c* axis to form a supramolecular layer structure in an –ABAB– packing fashion.

The most unusual feature is the packing motif of the supramolecular layer, as shown in Figure 4. The supramolecular layers stack to form a 3D supramolecular structure along the *a*–*c* axes. Note that there exist large spaces between any two adjacent layers, which are filled by $\{PMo_{12}Sb_2O_{40}\}$ POMs. The packing motif of the POMs in **3**, shown in Figure 4, is also interesting, exhibiting a body-centred lattice.

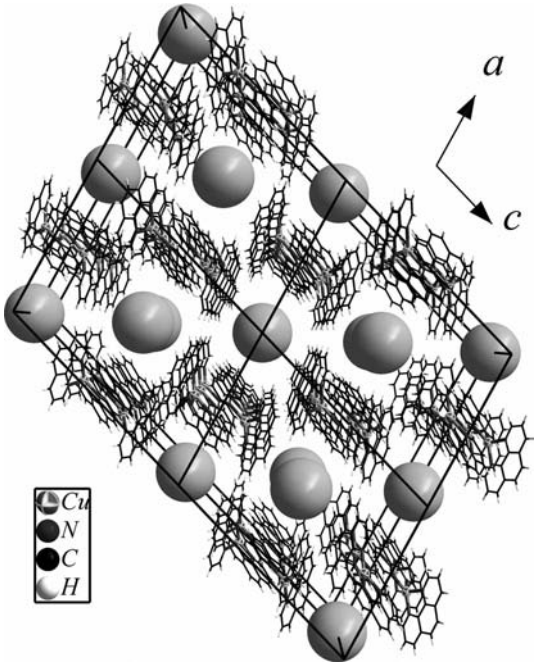

Figure 4. Representation of the packing motif of compound **3**. The large balls represent the $[PMo_{12}Sb_2O_{40}]^{3-}$ POMs.

There also exist extensive hydrogen-bonding interactions between carbon atoms of the Phen ligands and oxygen atoms of the polyoxoanions $[PMo_{12}Sb_2O_{40}]^{3-}$, as in compounds **1** and **2**. These complex hydrogen bonds connect the $[PMo_{12}Sb_2O_{40}]^{3-}$ POMs and $[Cu(Phen)_2]^+$ TMCs to form a 3D supramolecular structure. These hydrogen bonds are listed in Table S1.

Crystal Structure of 4

The asymmetric unit of **4** contains half of a $[PMo_{12}Sb_2O_{40}]^{3-}$ with the pseudo-Keggin configuration, a $[Cd(bpy)(bpy)_{0.5}(H_2O)]^{2+}$ TMC, a dissociated bpy and a water molecule. The polyanion $[PMo_{12}Sb_2O_{40}]^{3-}$ is identical to that of **3** with the only differences being in their bond lengths and angles. The results of BVSs (Table S2) reveal that the formula of the $\{PMo_{12}Sb_2O_{40}\}$ in **4** is $[PMo^{V}_{5}Mo^{VI}_{7}Sb^{III}_{2}O_{40}]^{2-}$.[13]

Compound **4** contains TMC $[Cd(bpy)(bpy)_{0.5}(H_2O)]^{2+}$, but its role is very different to that of the TMCs of compounds **1**–**3**. The TMCs in compounds **1**–**3** are all "independent" of each other, that is, they do not show covalent interactions between each other. However, the TMCs in **4** are building blocks of a 1D transition-metal coordination chain structure. As shown in Figure 5, the Cd(1) ion of **4** is coordinated by four nitrogen atoms of four bpy ligands (two N3 bpy and two N1 bpy ligands) in the equatorial plane and two oxygen atoms of water molecules in the axial positions. The Cd–N bond lengths [2.35(2)–2.38(2) Å] are comparable to the Cd–O bond lengths [2.35(2) Å]. The two N3 bpy ligands are bidentate and act as bridges interconnecting the Cd(1) ions to form a 1D coordination chain structure along the *b* axis, whereas the other two N1 bpy ligands are monodentate, that is, only one nitrogen atom of the N1 bpy ligand coordinates to the Cd(1) centre, which means that the other nitrogen atom of the N1 bpy has no covalent interactions with any metal atom. Thus, a 1D chain coordination polymer was formed.

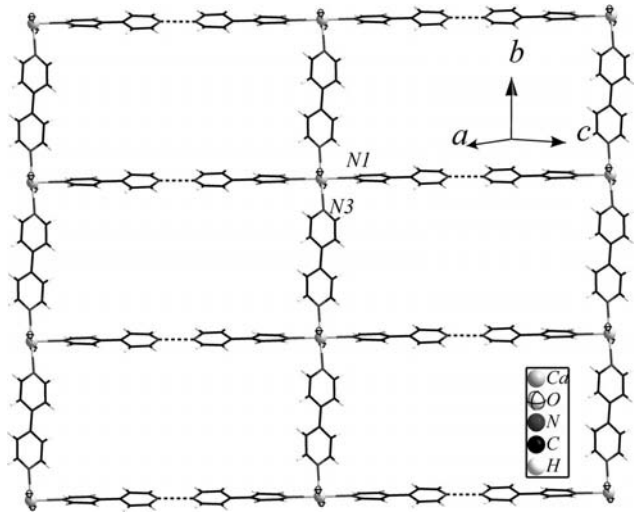

Figure 5. Combined ball-and-stick and wire representation of the grid-like layer structure of compound **4**.

It is interesting that the 1D chains are arranged in parallel along the *a*–*c* axis. Detailed analysis revealed that the uncoordinated nitrogen atom N2 of the N1 bpy ligand of the 1D chain interacts with the N2 atom of the N1 bpy of an adjacent 1D chain through strong interactions with a N···N distance of 2.66(3) Å. As shown in Figure 5, 1D chains are linked through the interactions of N···N atoms to form a novel 2D grid-like layer structure.

Another unusual feature of compound **4** is that the 2D grid-like layers are stacked along the *a* + *c* axis to form a 3D supramolecular structure, as shown in Figure 6. Just like compound **3**, there exist large spaces between any two adjacent supramolecular layers, but in contrast to compound **3**, the spaces are filled not only by $\{PMo_{12}Sb_2O_{40}\}$ POMs, but also by dissociated bpy ligands, as shown in Figure 6.

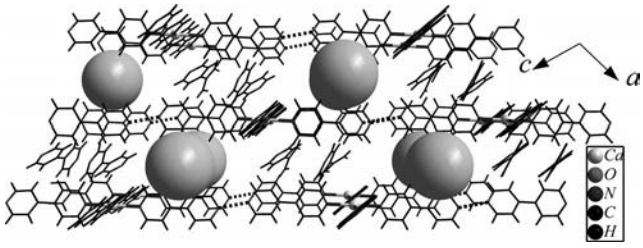

Figure 6. Representation of the packing motif of compound **4**. The large balls represent the $[PMo_{12}Sb_2O_{40}]^{3-}$ POMs.

Just as for compounds **1**, **2** and **3**, there exist extensive hydrogen-bonding interactions between carbon atoms of the bpy ligands and oxygen atoms of the polyoxoanions $[PMo_{12}Sb_2O_{40}]^{3-}$. These complex hydrogen bonds connect the $[PMo_{12}Sb_2O_{40}]^{3-}$ POMs, the 1D chain coordination polymers and dissociated bpys to form a 3D supramolecular structure. These hydrogen bonds are listed in Table S1.

Keggin anions ($\{PMo_{12}O_{40}\}$ or $\{PW_{12}O_{40}\}$) can generally accept up to four electrons.[16] There is one Keggin derivative that accepts up to six electrons,[17] several derivatives that accept up to eight electrons[18] and even one derivative that accepts up to 12 electrons.[19] The bis-antimony-capped pseudo-Keggin polyoxoanion $\{PMo_{12}Sb_2O_{40}\}$ in compounds $[PMo_{12}Sb_2O_{40}][Cu(enMe)_2]\cdot 4H_2O$, $[PMo_{12}Sb_2O_{40}][Ni(enMe)_2]\cdot 4H_2O$ and $[PMo_{12}Sb_2O_{40}][Cu(en)_2]\cdot H_3O\cdot H_2O$ all accept up to five electrons.[9f] The bis-antimony-capped α-Keggin polyoxoanion in **1**, **3** and **4** accepts five electrons just like the pseudo-Keggin polyoxoanion. However, the bis-antimony-capped α-Keggin polyoxoanion in **2** accepts up to six electrons and the bis-antimony-capped α-Keggin polyoxoanion in compound $[H_4PMo_{12}Sb_2O_{40}](Im)_2\cdot 2H_2O$ (Im = imidazole) that was reported recently accepts up to seven electrons.[12b] The stabilization of these highly reduced species comes from the positively charged capping ions (lanthanide or transition-metal ions or antimony).

XPS Spectroscopy

The XPS spectrum of compound **1** in the Cu 2P region presents a peak at 933.1 eV, which can be ascribed to Cu^+ (Figure S3).[20] The XPS spectrum in the Sb 3d region presents two peaks at 540.1 and 530.7 eV, which can be ascribed to Sb^{3+} (see Figure S1 in the Supporting Information).[20] The XPS spectrum in the Mo 3d region presents four overlapping peaks at 236.2, 234.7, 232.9 and 231.6 eV, respectively, which can be ascribed to the mixture of Mo^{5+} and Mo^{6+} (Figure S3).[20] The XPS spectrum in the P 2P region presents a peak at 133.6 eV, which can be ascribed to P^{5+} (Figure S3).[20]

The XPS spectra of compounds **2**–**4** in the Mo 3d region present similar overlapping peaks at 236.0, 234.9, 232.8 and 231.7 eV for compound **2**, 236.3, 234.7, 232.8 and 231.6 eV for compound **3** and 236.5, 234.7, 232.9 and 231.6 eV for compound **4**, which can be ascribed to the mixture of Mo^{5+} and Mo^{6+} in compounds **2**–**4** (Figures S4–S6).[20] The XPS spectra in the Sb 3d region present analogous peaks at 540.0 and 530.7 eV for compound **2**, 539.9 and 530.7 eV for compound **3** and 540.0 and 530.7 eV for compound **4**, which can be ascribed to Sb^{3+} in compounds **2**–**4** (Figures S4–S6).[20] The XPS spectra in the P 2p region present analogous peaks at 134.0 eV for compound **2**, 133.9 eV for compound **3** and 134.4 eV for compound **4**, which can be ascribed to P^{5+} in compounds **2**–**4** (Figures S4–S6).[20] In addition, the XPS spectra in the Cd 3d region present analogous peaks at 415.7 and 399.3 eV for compound **2** and 415.0 eV for compound **3**, which can be ascribed to Cd^{2+} in compounds **2** and **3** (Figures S4 and S5). The XPS spectrum for compound **4** in the Cu 2P region presents a peak at 931.8 eV, which can be ascribed to Cu^+ in compound **4** (Figure S6).[20]

XRD Analysis

The powder X-ray diffraction patterns for **1**–**4** are in good agreement with those simulated based on the data of the single-crystal structures (as shown in Figures S7–S10). The differences in reflection intensity are probably due to preferred orientations in the powder samples of compounds **1**–**4**.

UV/Vis Spectrophotometry

The UV/Vis spectra of **1**–**4** in the range 256–500 nm are shown in Figure S11. The spectra show two characteristic bands for ligand-to-metal (Mo) charge transfer in the polyanions of **1**, **2** and **4**. The bands corresponding to the $p_\pi(O_d)\rightarrow d_{\pi^*}(Mo)$ transitions are centred at 257 (for **1**), 265 (for **2**) and 257 nm (for **4**). The shoulders at 318 (for **1**), 325 (for **2**) and 326 nm (for **4**) are assigned to the $p_\pi(O_{b,c})\rightarrow d_{\pi^*}(Mo)$ charge-transfer transition. However, the UV/Vis spectrum of compound **3** only exhibits one band centred at 261 nm assigned to the $p_\pi(O_d)\rightarrow d_{\pi^*}(Mo)$ transition; the shoulder band for compound **3** was not observed.

TG Analysis

The TG analyses of **1**–**4** in the range 35–800 °C are shown in Figures S12–S15. The TG curves for **1**, **2** and **4** are similar. The TG curve for **1** decreases until 495 °C with a weight loss of 11.66% (until 493 °C with a weight loss of 25.14% for **2** and until 505 °C with a weight loss of 26.71% for **4**), which is consistent with the release of the Im ligands and the oxidation of Sb^{3+} to Sb^{5+}, calculated to be 12.18% for **1** (consistent with the release of the Phen ligands and

the oxidation of Sb^{3+}, calculated to be 23.77% for **2**, and the release of the bpy ligands and water molecules and the oxidation of Sb^{3+}, calculated to be 27.08%). The curves increase from 495 to 664 °C for **1**, from 495 to 664 °C for **2** and from 505 to 680 °C for **4**, which correspond to the oxidation of Mo^{5+} to Mo^{6+}. The curves decreased sharply again from 710 °C for **1**, 713 °C for **2** and 708 °C for **4**, which corresponds to the sublimation of the MoO_3 in these compounds.

The TG curve of compound **3** is different to the others. The curve decreases until 607 °C, with a weight loss of 45.41%, which is consistent with the loss of the Phen ligands, sublimation of 4.5 MoO_3 and the oxidation of Sb^{3+} (calculated to be 45.87%). The curve increases again from 607 to 696 °C, which corresponds to the oxidation of the Mo^{5+} atoms in compound **3**. The curve then decreases sharply again from 710 °C, which corresponds to the sublimation of MoO_3.

Conclusions

Four new structures based on bis-antimony-capped Keggin polyoxoanion $\{PMo_{12}Sb_2O_{40}\}$ have been synthesized and structurally characterized. Compound **1** exhibits a novel 1D structure, compound **2** is the first example of an extended structure constructed from polyoxoanions, transition-metal coordination complexes and halide ions and compounds **3** and **4** are supramolecular structures constructed from $\{PMo_{12}Sb_2O_{40}\}$ polyoxoanions and different transition-metal coordination fragments. Further research is underway to determine the rules of their synthesis and to explore their attractive properties.

Experimental Section

General: All chemicals used were reagent grade and used without further purification. C,H,N elemental analyses were carried out with a Perkin–Elmer 2400 CHN elemental analyzer and metal contents were determined by inductively coupled plasma (ICP) analyses with a Perkin–Elmer Optima 3300DV ICP spectrometer. Infrared spectra were recorded as KBr pellets with a Perkin–Elmer SPECTRUM ONE FTIR spectrometer. The TG curves were obtained by using a Perkin–Elmer TGA-7000 thermogravimetric analyser in flowing air with a temperature ramp rate of 10 °C min^{-1}. XPS analyses were performed with a Thermo ESCALAB 250 spectrometer with an Mg-K_α (1253.6 eV) achromatic X-ray source. The UV/Vis spectra were recorded with a Shimadzu UV3100 spectrophotometer as saturated solutions of *N*,*N*-dimethylformamide.

$\{[PMo_{12}Sb_2O_{40}][Cu(Im)_2]_2\}\cdot Im$ (1): Compound **1** was synthesized hydrothermally by reaction of $(NH_4)_3PMo_{12}O_{40}\cdot xH_2O$ ($M_r \approx$ 1876.34, 0.939 g, 0.5 mmol), $H_2C_2O_4\cdot 2H_2O$ (0.252 g, 2.0 mmol), Sb_2O_3 (0.294 g, 1 mmol), $CuCl_2\cdot 2H_2O$ (0.187 g, 1.1 mmol), Im (0.14 g, 2.0 mmol) and distilled water (18 mL) in a 20mL Teflon-lined autoclave. The pH of the mixture was necessarily adjusted to 4 with $NH_3\cdot H_2O$ solution. The mixture was heated under autogenous pressure at 160 °C for 4 d and then left to cool to room temperature. Dark block crystals were isolated in a yield of about 60% (based on Mo). IR (as shown in Figure S16): $\tilde{\nu}$ = 1581, 1539, 1423, 1256, 1175, 1071, 948, 725, 624, 607, 511, 476 cm^{-1}. $C_{15}H_{20}Cu_2Mo_{12}N_{10}O_{40}PSb_2$ (2533.28): calcd. C 7.11, H 0.80, N 5.53, P 1.22, Mo 45.45, Sb 9.61, Cu 5.02; found C 7.08, H 0.49, N 5.34, P 1.29, Mo 45.24, Sb 9.32, Cu 4.85.

$\{[PMo_{12}Sb_2O_{40}][(Cd(Phen)_2)_2Cl]\}$ (2): Compound **2** was synthesized hydrothermally by reaction of $(NH_4)_3PMo_{12}O_{40}\cdot xH_2O$ (0.937 g, 0.5 mmol), $H_2C_2O_4\cdot 2H_2O$ (0.252 g, 2.0 mmol), Sb_2O_3 (0.294 g, 1 mmol), $CdCl_2\cdot 2.5H_2O$ (0.228 g, 1.0 mmol), Phen·H_2O (0.197 g, 1.0 mmol) and distilled water (18 mL) in a 20mL Teflon-lined autoclave. The pH of the mixture was necessarily adjusted to 4.5 with $NH_3\cdot H_2O$ solution. The mixture was heated under autogenous pressure at 160 °C for 4 d and then left to cool to room temperature. Dark block crystals were isolated in a yield of about 65% (based on Mo). IR (as shown in Figure S17): $\tilde{\nu}$ = 1617, 1516, 1427, 1142, 1103, 1056, 961, 842, 793, 765, 723, 635, 506 cm^{-1}. $C_{48}H_{32}Cd_2ClMo_{12}N_8O_{40}PSb_2$ (3046.82): calcd. C 18.92, H 1.06, N 3.68, P 1.02, Mo 37.79, Sb 7.99, Cd 7.38; found C 18.49, H 1.30, N 3.34, P 1.29, Mo 37.72, Sb 7.33, Cd 7.50.

$[Cu(Phen)_2]_2[PMo_{12}Sb_2O_{40}]$ (3): Compound **3** was synthesized hydrothermally by reaction of $(NH_4)_3PMo_{12}O_{40}\cdot xH_2O$ (0.937 g, 0.5 mmol), $H_2C_2O_4\cdot 2H_2O$ (0.253 g, 2.0 mmol), Sb_2O_3 (0.291 g, 1 mmol), $CuCl_2\cdot 2H_2O$ (0.170 g, 1.0 mmol), Phen·H_2O (0.198 g, 1.0 mmol) and distilled water (18 mL) in a 20mL Teflon-lined autoclave. The pH of the mixture was necessarily adjusted to 4 with $NH_3\cdot H_2O$ solution. The mixture was heated under autogenous pressure at 160 °C for 5 d and then left to cool to room temperature. Dark block crystals were isolated in a yield of about 60% (based on Mo). IR (as shown in Figure S18): $\tilde{\nu}$ = 1620, 1420, 1133, 951, 837, 723, 631, 510, 421 cm^{-1}. $C_{48}H_{32}Cu_2Mo_{12}N_8O_{40}PSb_2$ (2913.65): calcd. C 19.79, H 1.11, N 3.85, P 1.06, Mo 39.51, Sb 8.36, Cu 4.36; found C 19.23, H 1.02, N 3.54, P 1.01, Mo 39.64, Sb 8.12, Cu 4.15.

$[Cd(bpy)_4(H_2O)_2][PMo_{12}Sb_2O_{40}]\cdot[bpy]\cdot 2H_2O$ (4): Compound **4** was synthesized hydrothermally by reaction of $(NH_4)_3PMo_{12}O_{40}\cdot xH_2O$ (0.502 g, 0.27 mmol), $H_2C_2O_4\cdot 2H_2O$ (0.253 g, 2.0 mmol), Sb_2O_3 (0.291 g, 1 mmol), $CdCl_2\cdot 2.5H_2O$ (0.278 g, 1.2 mmol), 4,4′-bpy·$2H_2O$ (0.192 g, 1.0 mmol) and distilled water (18 mL) in a 20mL Teflon-lined autoclave. The pH of the mixture was necessarily adjusted to 5.5 with $NH_3\cdot H_2O$ solution. The mixture was heated under autogenous pressure at 160 °C for 5 d and then left to cool to room temperature. Dark block crystals were isolated in a yield of about 65% (based on Mo). IR (as shown in Figure S19): $\tilde{\nu}$ = 1601, 1531, 1468, 1404, 1320, 1214, 1064, 1009, 942, 805, 725, 626, 580, 513, 478, 439 cm^{-1}. $C_{50}H_{48}CdMo_{12}N_{10}O_{44}PSb_2$ (3031.16): calcd. C 19.81, H 1.60, N 4.62, P 1.02, Mo 37.98, Sb 8.03, Cd 3.71; found C 19.08, H 1.49, N 4.34, P 1.29, Mo 37.24, Sb 8.32, Cd 3.85.

X-ray Crystallography: All the reflection intensity data for **1**–**4** were collected with a Bruker Apex II diffractometer equipped with graphite-monochromated Mo-K_α (λ = 0.71073 Å) radiation at room temperature. The structures of **1**–**4** were solved by direct methods and the four structures were further refined by using the full-matrix least-squares methods on F^2 using the SHELXTL-97 crystallographic software package. Anisotropic thermal parameters were refined for all the non-hydrogen atoms in **1**–**4**. All the hydrogen atoms of the ligands were placed in geometrically calculated positions and refined with fixed isotropic displacement parameters using a riding model except for the lattice water molecules in compound **4**. A summary of the crystallographic data and structure refinements for **1**–**4** is provided in Table 1.

CCDC-782927 (for **1**), -782928 (for **2**), -797253 (for **3**) and -797254 (for **4**) contain the supplementary crystallographic data for this paper. These data can be obtained free of charge from The Cam-

Table 1. Crystal data and structure refinement for **1**–**4**.

	$C_{15}H_{20}Cu_2Mo_{12}N_{10}O_{40}PSb_2$	$C_{48}H_{32}Cd_2ClMo_{12}N_8O_{40}PSb_2$	$C_{48}H_{32}Cu_2Mo_{12}N_8O_{40}PSb_2$	$C_{50}H_{48}CdMo_{12}N_{10}O_{44}PSb_2$
M_r	2533.28	3046.82	2913.65	3031.16
Crystal system	triclinic	orthorhombic	monoclinic	triclinic
Space group	$P\bar{1}$	*Pccn*	$P2_1/n$	$P\bar{1}$
a [Å]	10.6999(15)	16.549(2)	15.1489(9)	10.9094(9)
b [Å]	13.425(2)	20.499(3)	11.5637(9)	11.8217(9)
c [Å]	18.891(3)	20.850(5)	20.8968(14)	15.4840(11)
α [°]	109.481(9)	90	90	90.342(5)
β [°]	92.030(7)	90	107.637(4)	107.225(5)
γ [°]	102.335(13)	90	90	92.522(5)
V [Å^3]	2482.4(6)	7073(2)	3488.6(4)	1905.1(3)
Z	2	4	2	1
D_c [gcm^{-3}]	3.389	2.861	2.774	2.642
μ [mm^{-1}]	4.970	3.547	3.557	2.995
F(000)	2357	5720	2750	1438
Data/parameters	12199/739	8720/516	8735/529	8953/562
Gof	1.004	1.089	0.996	1.169
R_1[a] [$I>2\sigma(I)$]	0.0398	0.0786	0.0433	0.1060
wR_2[b] (all data)	0.1166	0.2870	0.1274	0.2875

[a] $R_1 = \Sigma||F_o| - |F_c||/\Sigma|F_o|$. [b] $wR_2 = \{\Sigma[w(F_o^2 - F_c^2)^2]/\Sigma[w(F_o^2)^2]\}^{1/2}$.

bridge Crystallographic Data Centre via www.ccdc.cam.ac.uk/data_request/cif.

Supporting Information (see footnote on the first page of this article): Wire and ellipsoid representations of the $\{Cd(Phen)_2\}_2Cl\}^{3+}$ "butterfly" cluster, combined ball-and-stick and wire representation of the packing motif of copper dimers in **3**, XPS spectra, XRD analyses, UV/Vis specta, TG analyses and IR spectra for **1**–**4**.

Acknowledgments

This work was supported by the National Natural Science Foundation of China (NSFC) (grant number 21003056). We also thank Jilin University for a grant (grant number 200903123).

[1] M. T. Pope, *Heteropoly and Isopoly Oxometalates*, Springer, Berlin, **1983**.
[2] M. T. Pope, A. Müller, *Angew. Chem. Int. Ed. Engl.* **1991**, *30*, 34–48.
[3] M. T. Pope, A. Müller, *Polyoxometalates: From Platonic Solids to Anti-Retro Viral Activity*, Kluwer, Dordrecht, The Netherlands, **1994**.
[4] For a review on polyoxometalates, see: C. Hill, *Chem. Rev.* **1998**, *98*, 1–2.
[5] M. T. Pope, A. Müller, *Polyoxometalate Chemistry: From Topology* via *Self-Assembly to Applications*, Kluwer, Dordrecht, The Netherlands, **2001**.
[6] T. Yamase, M. T. Pope, *Polyoxometalate Chemistry for Nano-Composite Design*, Kluwer, Dordrecht, The Netherlands, **2002**.
[7] a) M. I. Khan, E. Yohannes, R. J. Doedens, *Angew. Chem. Int. Ed.* **1999**, *38*, 1292–1294; b) J. Lu, Y. Xu, N. K. Goh, L. S. Chia, *Chem. Commun.* **1998**, 2733–2734; c) A. Tripathi, T. Hughbanks, A. Clearfield, *J. Am. Chem. Soc.* **2003**, *125*, 10528–10529; d) J. R. D. Debord, R. C. Haushalter, L. M. Meyer, D. J. Rose, P. J. Zapf, J. Zubieta, *Inorg. Chim. Acta* **1997**, *256*, 165–168; e) P. J. Hagrman, D. Hagrman, J. Zubieta, *Angew. Chem. Int. Ed.* **1999**, *38*, 2638–2684; f) D. Hagrman, C. Zubieta, D. J. Rose, J. Zubieta, R. C. Haushalter, *Angew. Chem. Int. Ed. Engl.* **1997**, *36*, 873–876; g) A. Dolbecq, P. Mialane, L. Lisnard, J. Marrot, F. Sécheresse, *Chem. Eur. J.* **2003**, *9*, 2914–2920; h) P. Mialane, A. Dolbecq, F. Sécheresse, *Chem. Commun.* **2006**, 3477–3485; i) S. Reinoso, P. Vitoria, J. M. Gutiérrez-Zorrilla, L. Lezama, L. San Felices, J. I. Beitia, *Inorg. Chem.* **2005**, *44*, 9731–9742; j) J. Thomas, A. Ramanan, *Cryst. Growth Des.* **2008**, *8*, 3391; k) K. Pavani, S. E. Lofland, K. V. Ramanujachary, A. Ramanan, *Eur. J. Inorg. Chem.* **2007**, 568–578.
[8] a) C. Lei, J.-G. Mao, Y.-Q. Sun, J.-L. Song, *Inorg. Chem.* **2004**, *43*, 1964–1968; b) C. Liu, D. Zhang, M. Xiong, D. Zhu, *Chem. Commun.* **2002**, 1416–1417; c) Y.-P. Ren, X.-J. Kong, X.-Y. Hu, M. Sun, L.-S. Long, R.-B. Huang, L.-S. Zheng, *Inorg. Chem.* **2006**, *45*, 4016–4023; d) G.-C. Qu, L. Jiang, X.-L. Feng, T.-B. Lu, *Dalton Trans.* **2009**, 71–76; e) J.-Y. Niu, D.-J. Guo, J.-P. Wang, J.-W. Zhao, *Cryst. Growth Des.* **2004**, *4*, 241–247; f) S.-T. Zheng, J. Zhang, G.-Y. Yang, *Angew. Chem. Int. Ed.* **2008**, *47*, 3909–3913; g) J.-W. Zhao, C.-M. Wang, J. Zhang, S.-T. Zheng, G.-Y. Yang, *Chem. Eur. J.* **2008**, *14*, 9223–9239; h) B.-Z. Lin, S.-X. Liu, *Chem. Commun.* **2002**, 2126–2127.
[9] a) X.-B. Cui, J.-Q. Xu, H. Meng, S.-T. Zheng, G.-Y. Yang, *Inorg. Chem.* **2004**, *43*, 8005–8009; b) X.-B. Cui, Y.-Q. Sun, G.-Y. Yang, *Inorg. Chem. Commun.* **2003**, *6*, 259–261; c) C. Pan, J. Xu, G. Li, X. Cui, L. Ye, G. Yang, *Dalton Trans.* **2003**, 517–518; d) X.-B. Cui, J.-Q. Xu, Y. Li, Y.-H. Sun, G.-Y. Yang, *Eur. J. Inorg. Chem.* **2004**, 1051–1055; e) L.-J. Zhang, X.-L. Zhao, J.-Q. Xu, T.-G. Wang, *J. Chem. Soc., Dalton Trans.* **2002**, 3275–3276; f) S.-Y. Shi, Y. Chen, J.-N. Xu, Y. Wang, G.-W. Wang, X.-B. Cui, G.-D. Yang, J.-Q. Xu, *Dalton Trans.* **2010**, *39*, 1389–1394; g) S.-Y. Shi, Y.-C. Zou, X.-B. Cui, J.-N. Xu, Y. Wang, G.-W. Wang, G.-D. Yang, J.-Q. Xu, *CrystEngComm* **2010**, *12*, 2122–2128; h) S.-Y. Shi, Y. Chen, J.-N. Xu, Y.-C. Zou, X.-B. Cui, Y. Wang, T.-G. Wang, J.-Q. Xu, Z.-M. Gao, *CrystEngComm* **2010**, *12*, 1949–1954; i) S.-Y. Shi, C.-L. Pan, Y. Chen, X.-B. Cui, Y.-K. Lu, Y. Wang, J.-Q. Xu, *Inorg. Chem. Commun.* **2009**, *12*, 1124–1127; j) Y. Wang, L. Ye, T.-G. Wang, X.-B. Cui, S.-Y. Shi, G.-W. Wang, J.-Q. Xu, *Dalton Trans.* **2010**, *39*, 1916–1919.
[10] a) H.-Y. An, Y.-G. Li, E.-B. Wang, D.-R. Xiao, C.-Y. Sun, L. Xu, *Inorg. Chem.* **2005**, *44*, 6062–6070; b) H.-Y. An, E.-B. Wang, D.-R. Xiao, Y.-G. Li, Z.-M. Su, L. Xu, *Angew. Chem. Int. Ed.* **2006**, *45*, 904–908; c) J. Lü, E.-H. Shen, Y.-G. Li, D.-R. Xiao, E.-B. Wang, L. Xu, *Cryst. Growth Des.* **2005**, *5*, 65–67; d) C.-Y. Sun, Y.-G. Li, E.-B. Wang, D.-R. Xiao, H.-Y. An, L. Xu, *Inorg. Chem.* **2007**, *46*, 1541–1543; e) Y. Lu, Y. Xu, E.-B. Wang, X.-X. Xu, Y. Ma, *Inorg. Chem.* **2006**, *45*, 2055–2060; f) H.-Y. An, Y.-G. Li, D.-R. Xiao, E.-B. Wang, C.-Y. Sun, *Cryst. Growth Des.* **2006**, *6*, 1107–1112.
[11] a) P. Q. Zheng, Y. P. Ren, L. S. Long, R. B. Huang, L. S. Zheng, *Inorg. Chem.* **2005**, *44*, 1190–1192; b) X. L. Wang, C. Qin, E. B. Wang, Y. G. Li, N. Hao, C. W. Hu, L. Xu, *Inorg. Chem.* **2004**, *43*, 1850–1856; c) C. P. Pradeep, D. L. Long, G. N.

Newton, Y. F. Song, L. Cronin, *Angew. Chem. Int. Ed.* **2008**, *47*, 4388–4391; d) Z. H. Yi, X. B. Cui, X. Zhang, G. D. Yang, J. Q. Xu, X. Y. Yu, H.-H. Yu, W. J. Duan, *J. Mol. Struct.* **2008**, *891*, 123–128; e) T. R. Veltman, A. K. Stover, A. N. Sarjeant, K. M. Ok, P. S. Halasyamani, A. J. Norquist, *Inorg. Chem.* **2006**, *45*, 5529–5537; f) R. Atencio, A. Briéno, X. Galindo, *Chem. Commun.* **2005**, 637–639; g) R. Atencio, A. Bricéno, P. Silva, J. A. Rodríguez, J. C. Hanson, *New J. Chem.* **2007**, *31*, 33–38; h) Y. Wang, C. L. Pan, L. N. Xiao, F. Q. Wu, H. Ding, Y. B. Liu, Z. M. Gao, D. F. Zheng, T. G. Wang, G. D. Yang, X. B. Cui, J. Q. Xu, *J. Solid-State Chem.* **2010**, *183*, 2862–2868.

[12] a) Q.-B. Zhang, Y.-K. Lu, Y.-B. Liu, J. Lu, M.-H. Bi, J.-H. Yu, T.-G. Wang, J.-Q. Xu, J. Liu, *Inorg. Chem. Commun.* **2006**, *9*, 544–547; b) Y.-K. Lu, J.-N. Xu, X.-B. Cui, J. Jin, S.-Y. Shi, J.-Q. Xu, *Inorg. Chem. Commun.* **2010**, *13*, 46–49.

[13] I. D. Brown in *Structure and Bonding in Crystals* (Eds.: M. O'keeffe, A. Navrotsky), Academic Press, New York, **1981**, vol. 2, p. 1.

[14] S.-Y. Shi, Y. Wang, G.-W. Wang, X.-B. Cui, J.-Q. Xu, *Dalton Trans.* **2009**, 6099–6102.

[15] X. M. Lu, X. D. Shi, Y. G. Bi, C. Yu, Y. Y. Chen, Z. X. Chi, *Eur. J. Inorg. Chem.* **2009**, 5267–5276.

[16] Z.-P. Wang, S. Gao, L. Xu, E.-H. Shen, E.-B. Wang, *Polyhedron* **1996**, *15*, 1383–1388.

[17] Q. Chen, C. L. Hill, *Inorg. Chem.* **1996**, *35*, 2403–2405.

[18] a) L. M. Rodriguez-Albelo, A. R. Ruiz-Salvador, A. Sampieri, D. W. Lewis, A. Gómez, B. Nohra, P. Mialane, J. Marrot, F. Sécheresse, C. Mellot-Draznieks, R. N. Biboum, B. Keita, L. Nadjo, A. Dolbecq, *J. Am. Chem. Soc.* **2009**, *131*, 16078–16087; b) P. Mialane, A. Dolbecq, L. Lisnard, A. Mallard, J. Marrot, F. Sécheresse, *Angew. Chem. Int. Ed.* **2002**, *41*, 2398–2401.

[19] A. Müller, C. Beugholt, P. Kögerler, H. Bögge, S. Bud'ko, M. Luban, *Inorg. Chem.* **2000**, *39*, 5176–5177.

[20] C D. Wagner, W. M. Riggs, L. E. Davis, J. F. Moulder, G. E. Muilenberg, *Handbook of X-ray Photoelectron Spectroscopy*, Perkin–Elmer, Eden Prairie, MN, **1979**.

Received: November 17, 2010
Published Online: March 9, 2011

